PIDA Control of Heat Exchangers

Michele Schiavo[a] Manuel Beschi[a] Manuel G. Satué[b]
Manuel R. Arahal[b] Antonio Visioli[a*]

[a] Dipartimento di Ingegneria Meccanica e Industriale
University of Brescia, Brescia, Italy
e-mail: {michele.schiavo, manuel.beschi, antonio.visioli}@unibs.it

[b] Systems Engineering and Automation Department,
University of Seville, Seville, Spain
e-mail: {mgarrido16, arahal}@us.es

[*] corresponding author

This is the pre-peer reviewed version of the following article: PIDA Control of Heat Exchangers, which has been published in final form at DOI: 10.1109/ETFA61755.2024.10711147.

Abstract

Thermal Energy Storage (TES) systems represent a cornerstone in the development of sustainable energy solutions, enhancing the flexibility in energy management. Heat exchangers are pivotal components of TES systems and they require precise control to optimize efficiency. Proportional-Integral-Derivative (PID) controllers are commonly employed for heat exchangers control but, since these systems are subject to time-delays and nonlinearities, their performance leaves room for enhancement. This paper explores the potential of Proportional-Integral-Derivative-Acceleration (PIDA) control, also known as PIDD or PIDD^2, that introduces a double derivative (acceleration) component to the traditional PID structure. The capability of PIDA control in improving system performance compared to conventional PID controllers is evaluated through a simulation study performed on a realistic heat exchanger simulator. The obtained results show the efficacy of PIDA control in enhancing control performance without adding additional complexity or tuning efforts.

Index Terms: PIDA control, PID control, Tuning, Energy systems, Process control

1 Introduction

Thermal energy storage (TES) systems play a pivotal role in the development of sustainable energy solutions as they reduce the need of burning fossil fuels to generate heat. Indeed, they enable the efficient capture and re-utilization of waste heat by storing it as thermal energy in order to exploit it at a later stage in the plant [1], thus improving energy efficiency compared to the case where heat is just dissipated into the environment. Heat exchangers are key components of TES systems as they allow the transfer of thermal energy between different fluid streams, thus enabling heat distribution and storage. To ensure that the energy transfer is carried out in the most efficient and effective manner, thus maximizing the overall performance of the TES system, operational variables (such as flow rates and temperatures) must be maintained at their target values. Thus, closed-loop control of heat exchangers is fundamental.

As in many other process control applications, Proportional-Integral-Derivative (PID) control is the most widely employed technique for heat exchangers since it is low-cost, easy to implement and design (thanks to the availability of a large number of tuning rules), and it provides acceptable control performance in many applications. However, the dynamic behavior of heat exchangers is characterized by the presence of time-delays and nonlinearities that strongly limit the control performance achievable with PID control. This represents an issue in the context of TES systems where tight control specifications are required to maximize energy efficiency and, thus, the performance of a simple PID controller could be improved. For this reason, more advanced control methodologies have been proposed such as predictive functional control [2], fuzzy control [3], MPC [4], robust control [5] which, however, imply a greater complexity of the controller and of its tuning along with an increased cost. It would therefore be desirable to improve the control performance while maintaining the complexity of the controller and of its tuning unchanged with respect to a simple PID.

In this context, a promising option can be represented by Proportional-Integral-Derivative-Acceleration (PIDA) control (also known as PIDD or PIDD^2, which stands for Proportional-Integral-Double-Derivative) where the complexity of the PID structure is slightly increased by adding the double derivative of the feedback error in the calculation of the control action. The rationale is to add a zero in the transfer function of the controller, thus providing more phase lead to the system. This provides a performance improvement for high-order systems [6] and for integral processes [7–14]. On the other hand, the use of the PIDA structure implies an increment of the tuning effort since, with respect to PID, there is an additional parameter (namely, the acceleration gain or the second derivative time constant) that has to be selected. This shortcoming can be counteracted by providing tuning rules based on a process model that can be obtained by means of

a simple and cost-effective experiment. Advancements in this sense have been made in [15] and [16]. The first approach is based on Internal Model Control starting from a high-order process model estimated through the n-shifting technique based on a relay-feedback experiment [17]. The second approach employs a generalized Haalman tuning methodology based on a Third-Order-Plus-Dead-Time (TOPD) model obtained from an open-loop step response.
In this paper, the use of PIDA for heat exchangers control is considered. The goal is to evaluate whether PIDA can still bring a performance improvement with respect to PID also in the context where the process to be controlled is characterized by a distributed-lag dynamics and by a strong nonlinear behavior. To this end, a realistic nonlinear model of the heat exchanger is employed.
The paper is organized as follows: the case study considered and the heat exchanger model used for simulation are described in Section 2. The employed PIDA controller structure and the tuning methodology are described in Section 3. The obtained simulation results are presented in Section 4. Finally, conclusions are given in Section 5.

2 Case study

The case study considered in this work consists of a heat exchanger connected to a TES subsystem, as shown in Figure 1. A concentric tubes counterflow heat exchanger is used to cool a process fluid by means of a coolant fluid. The first one flows through the inner tube with a flow rate $F_p(t)$, while the second one flows in the outer tube with a flow rate $F_c(t)$. The coolant removes heat from the process fluid that, thus, enters the heat exchanger with an inlet temperature $T_{pi}(t)$ and leave it at an outlet temperature $T_{po}(t) < T_{pi}(t)$. In turn, the coolant enters the heat exchanger with an inlet temperature $T_{ci}(t)$ and leaves it at an outlet temperature $T_{co}(t) > T_{ci}(t)$. The heat removed from the process fluid by the coolant is then stored in a TES in order to be exploited according to the requirements of other parts of the plant (not shown in the figure). The control problem consists of regulating the process fluid outlet temperature $T_{co}(t)$ (process variable) by acting on the coolant flow rate $F_c(t)$ (control variable) by means of a pump. The values of $T_{pi}(t)$, $F_p(t)$ and $T_{ci}(t)$ depends on the operation of other parts of the plant and, thus, they can be seen as disturbances.

2.1 Heat exchanger model

In order to simulate the heat exchanger dynamic behavior, the realistic nonlinear model proposed in [18] is considered. The model is obtained by considering the overall heat exchanger as an array of cells, which can be

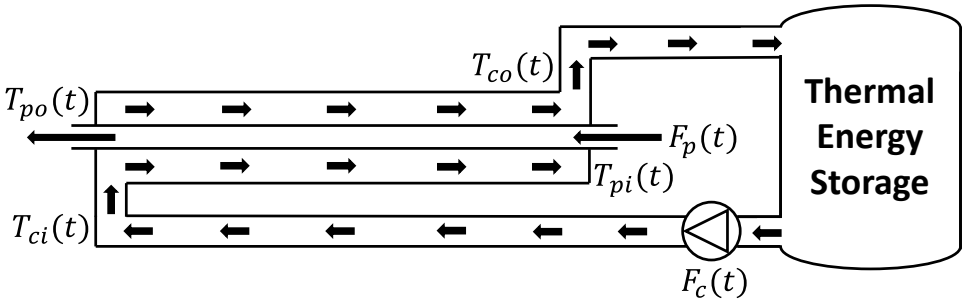

Figure 1: Diagram of the considered heat exchanger connected to a TES subsystem.

seen as small counterflow heat exchangers connected in series. A schematic representation of the jth cell is shown in Figure 2 where M_{p_j} and M_{c_j} are, respectively, the masses of process fluid and coolant contained in the cell. Their values are obtained by dividing the overall masses of process fluid (M_p) and of coolant (M_c) contained in the overall heat exchanger by the number of cells in which it has been divided. For each cell, the following differential equations can be obtained from the energy balance:

$$\frac{dT_{c_j}}{dt} = \frac{F_c}{M_{c_j}}\left(T_{c_{j-1}} - T_{c_j}\right) + \frac{UA}{M_c C_{p_c}}\Delta T_{lm_j} \tag{1}$$

$$\frac{dT_{p_j}}{dt} = \frac{F_p}{M_{p_j}}\left(T_{p_{j-1}} - T_{p_j}\right) - \frac{UA}{M_p C_{p_p}}\Delta T_{lm_j} \tag{2}$$

$$\Delta T_{lm_j} = \frac{\left(T_{c_j} - T_{p_{j+1}}\right) - \left(T_{c_{j-1}} - T_{p_j}\right)}{ln\frac{\left(T_{c_j} - T_{p_{j+1}}\right)}{\left(T_{c_{j-1}} - T_{p_j}\right)}} \tag{3}$$

where U is the overall heat transfer coefficient of the heat exchanger, A is the exchange surface of the heat exchanger, C_{p_c} is the specific heat of the coolant, C_{p_p} is the specific heat of the process fluid and ΔT_{lm_j} is the standard logarithmic mean temperature of the cell. Note that, in the equations, the dependency on time has been omitted, for the sake of brevity. The heat exchanger has been divided in 20 cells, which corresponds to as many pairs of differential equations. Note that the cells $j = 1$ and $j = 20$ correspond to the process fluid outlet and inlet, respectively. Hence, $T_{c_0}(t) = T_{ci}(t)$, $T_{p_{21}}(t) = T_{pi}(t)$ and $T_{c_{20}}(t) = T_{co}(t)$, while $T_{po}(t) = T_{p_1}(t - 36s)$, because of the presence of a time delay on the output due to the position of the outlet temperature sensor. The model parameters are shown in Table 1. Note that, since the model is nonlinear, its behavior depends on the inputs values, which define the operating point. In this case study, the nominal operating point defined by the combination of inputs shown in Table 2 is considered, as in [18]. Figure 3 shows the open-loop responses of the model

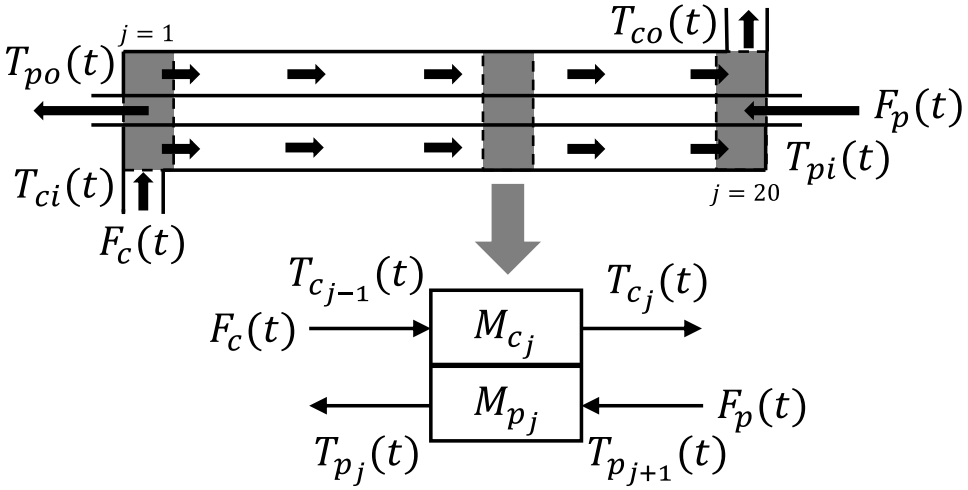

Figure 2: Schematic representation of the cell-based heat exchanger model considered.

Table 1: Model parameters.

Parameter	Value	Unit
U	198.74	W/(m^2 K)
A	1.86	m^2
C_{p_c}	1060.66	J/(kg K)
C_{p_p}	883.88	J/(kg K)
M_p	6.80	kg
M_c	18.14	kg

output $T_{co}(t)$, obtained by applying step changes to the control action $F_c(t)$, to highlight the strongly nonlinear behavior of the system. The simulations are performed starting from the nominal operating point. At time zero the system is perturbed by adding a step change of amplitude ΔF_c to the nominal control action $\overline{F_c} = 0.315$ kg/s. A representative set of symmetrical step changes is considered, namely $\Delta F_c = \pm 0.025$ kg/s, $\Delta F_c = \pm 0.05$ kg/s, $\Delta F_c = \pm 0.1$ kg/s and $\Delta F_c = \pm 0.15$ kg/s. These particular values are arbitrarily chosen inside the operative range of the considered heat exchanger to highlight the asymmetrical behavior of $T_{co}(t)$, which becomes more evident as the amplitude of ΔF_c increases. This suggests that the system gain varies nonlinearly with respect to $F_c(t)$. Note that the system has a negative gain, hence when a positive ΔF_c is applied the output $T_{co}(t)$ decreases, and viceversa.

Table 2: Inputs of the heat exchanger corresponding to its nominal operating point.

Parameter	Value	Unit
$\overline{F_p}$	0.189	kg/s
$\overline{F_c}$	0.315	kg/s
$\overline{T_{pi}}$	366.48	K
$\overline{T_{ci}}$	310.93	K

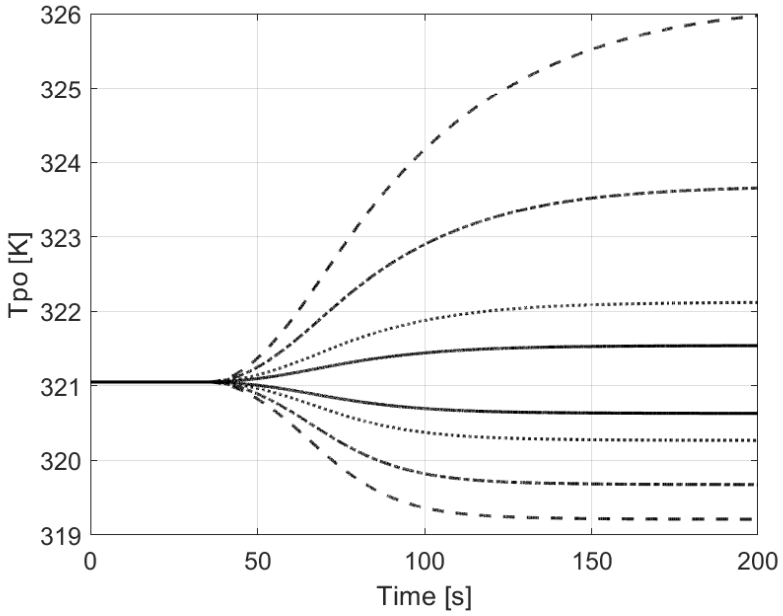

Figure 3: Open-loop process responses to symmetrical step changes of amplitude $\Delta F_c = \pm 0.025$ kg/s (solid line), $\Delta F_c = \pm 0.05$ kg/s (dotted line), $\Delta F_c = \pm 0.1$ kg/s (dashed-dotted line) and $\Delta F_c = \pm 0.15$ kg/s (dashed line), added to $\overline{F_c}$ at time zero.

3 Methodology

3.1 Linear model identification

In order to design the controller, a Third-Order-Plus-Dead-Time (TOPDT) model of the process is determined by evaluating an open-loop step response according to the method proposed in [19]. In particular, the process gain K is obtained as the ratio between the steady-state variation of the process variable and the amplitude of the input step. Then, the time instants t_5, t_{35} and t_{85} when the output, respectively, achieves 5%, 35% and 85% of its final value are determined. Then, the process transfer function is finally written as:

$$\hat{P}(s) = \frac{K}{(1+\tau s)\left(1+\frac{(1-\alpha)L}{2}s\right)^2} e^{-\alpha L s} \tag{4}$$

where

$$\begin{aligned} L &= 1.3t_{35} - 0.29t_{85} \\ \tau &= 0.67(t_{85} - t_{35}) \\ \alpha &= 0.598 + 0.4799\frac{t_5}{L} - \frac{0.41}{\left(\frac{t_5}{\tau}\right)^{0.6}} \end{aligned} \tag{5}$$

Note that, since the process exhibits nonlinear behavior, the amplitude of the input step on $F_c(t)$ has been appropriately chosen such that the response could be locally approximated as linear. More details regarding model identification are given in Section 4.

3.2 Controller structure

A block diagram of the considered closed-loop system is shown in Figure 4 where $\overline{T_{po}}(t)$ is the process fluid outlet temperature set-point, $\widetilde{T_{po}}(t)$ is the process fluid outlet temperature affected by the measurement noise $n(t)$ and $e(t)$ is the control error. Note that $T_{ci}(t)$, $T_{pi}(t)$ and $F_p(t)$ act as disturbances. We select $C(s)$ as a PIDA controller whose transfer function is

$$C(s) = K_p\left(1 + \frac{1}{T_i s} + T_d s + T_a s^2\right) \tag{6}$$

where K_p is the proportional gain, T_i is the integral time constant, T_d is the derivative time constant and T_a is the acceleration (double derivative) time constant.

Actually, in order to obtain a realizable controller, a first-order filter has to be added to the derivative action and a second-order filter has to be added

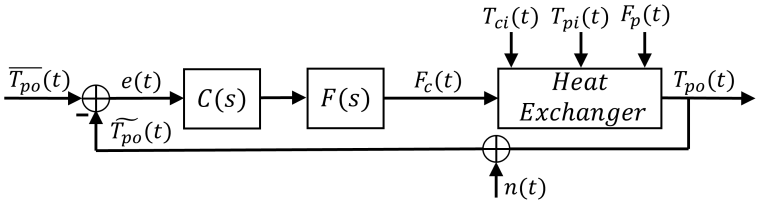

Figure 4: Block diagram of the closed-loop system.

to the acceleration action, yielding:

$$C(s) = K_p \left(1 + \frac{1}{T_i s} + \frac{T_d s}{\frac{T_d}{N} s + 1} + \frac{T_a s^2}{\left(\frac{T_a}{M} s + 1\right)^2} \right) \tag{7}$$

Moreover, these filters are also necessary to effectively filter the measurement noise and to avoid derivative and acceleration kicks. It is then worth noting that, if $T_a = 0$, then a standard PID controller results. Finally, to provide a better filtering of the measurement noise, the controller output is filtered with a low-pass filter defined as:

$$F(s) = \frac{1}{T_f s + 1} \tag{8}$$

where T_f is the time constant of the filter.

3.3 Controller tuning

The parameters of the PIDA controller can be selected by applying the generalized Haalman tuning proposed in [16], which is here briefly reviewed for the sake of clarity. After rewriting transfer function (4) as

$$\hat{P}(s) = \frac{K}{a_3 s^3 + a_2 s^2 + a_1 s + 1} e^{-\alpha L s} \tag{9}$$

where

$$\begin{aligned} a_3 &= L^2 \tau \left(\frac{\alpha}{2} - \frac{1}{2} \right)^2 \\ a_2 &= L^2 \left(\frac{\alpha}{2} - \frac{1}{2} \right)^2 - 2L\tau \left(\frac{\alpha}{2} - \frac{1}{2} \right) \\ a_1 &= \tau - 2L \left(\frac{\alpha}{2} - \frac{1}{2} \right) \end{aligned} \tag{10}$$

the integral, derivative and acceleration time constants are determined by applying a pole-zero cancellation considering (6), so that

$$\begin{aligned} T_i &= a_1 \\ T_d &= \frac{a_2}{a_1} \\ T_a &= \frac{a_3}{a_1} \end{aligned} \tag{11}$$

Then, as it is typically done in process control, the parameters of the filters are selected as $M = N = 10$ and the proportional gain K_p of (7) is calculated with a simple numerical procedure in order to obtained a convenient value of the maximum sensitivity, defined as

$$M_s := \max_{\omega \in [0,+\infty)} \left| \frac{1}{1 + C(j\omega)\hat{P}(j\omega)} \right|. \tag{12}$$

Finally, the time constant of the output filter is set as:

$$T_f = \frac{0.05}{\omega_{gc}} \tag{13}$$

where ω_{gc} is the gain crossover frequency of the loop transfer function $C(s)\hat{P}(s)$, that is the frequency for which $|C(j\omega_{gc})\hat{P}(j\omega_{gc})| = 1$.

4 Simulation results

To perform the simulations, the realistic nonlinear model described in Section 2.1 is used by considering the initial operating point resulting from the set of inputs shown in Table 2. First, the PIDA controller tuning is performed. To identify the TOPDT model, a step change of ΔF_c = -0.05 kg/s is applied to $F_c(t)$, which is therefore reduced from its nominal value of 0.315 kg/s to the final value of 0.265 kg/s. From the resulting outlet temperature open-loop response the TOPDT model is identified by applying the procedure described in Section 3.1 obtaining the following model parameters: $K = -21.45$ (K s)/kg, $L = 55.96$ s, $\alpha = 0.68$ and $\tau = 29.61$ s. On the basis of the identified model parameters, the three time constants of the PIDA are calculated according to (10) and (11). Then, the value of the proportional gain is determined after having fixed a desired value of the maximum sensitivity M_s equal to 1.4 in order to ensure the robustness with respect to the nonlinear behavior of the process. Finally, the value of the controller output filter time constant is determined according to (13).
In this simulation study, the performance of the PIDA controller are compared with those of a PID controller. The latter is tuned by following a

tuning procedure analogous to that used for the PIDA controller to ensure that a fair comparison is obtained. The only difference consists in the fact that, in the case of PID, the pole-zero cancellation technique used to determine the controller time constants (described in Section 3.3 for the PIDA controller) is that used in the standard Haalman method [20] which is based on the estimation of a Second-Order-Plus-Dead-Time (SOPDT) model. To obtain this model, the iterative procedure described in [21] is employed. Note that also this procedure is based on the same open-loop response used to tune the PIDA controller. As regards noise filtering the same rationale used for the PIDA controller is used. In particular, $N = 10$ is selected for the filter on the derivative action and (13) is used to determine the value of the output filter time constant. The resulting values of the tuning parameters for both controllers are summarized in Table 4.
The performance of the controllers is quantified by means of the integrated absolute error (IAE), defined as:

$$IAE = \int_0^{T_{sim}} |\overline{T_{po}}(t) - T_{po}(t)|dt \tag{14}$$

where T_{sim} is the simulation time, which is equal to 1000 s. Moreover, to better highlight the performance difference in terms of IAE between the two controllers the percentage difference Δ_{IAE} is defined as:

$$\Delta_{IAE} = \frac{IAE_{PID} - IAE_{PIDA}}{IAE_{PID}} * 100 \tag{15}$$

where IAE_{PID} and IAE_{PIDA} are the values of the IAE obtained with the PID and with the PIDA controllers, respectively. Measurement noise is simulated by applying to the signal n random values in the range [-0.5,0.5], thus equal to the 10% of the maximum set-point step amplitude applied to $\widetilde{T_{po}}(t)$. The performance of the controller has been assessed for both set-point following and disturbance rejection tasks. In particular, four different simulation scenarios are considered and, for each of them, different values of set-point changes or of disturbance amplitudes have been considered to assess the effect of nonlinearities on control performance. For each scenario, the simulation is started from the nominal operating point resulting from the set of inputs given in Table 2. The simulations start from a steady-state condition, hence $\overline{T_{po}}(t)$ is set equal to the process fluid output given by the nominal operating point, that is $T_{po}(t) = 321.05$ K. Moreover, the integral terms of both controllers are preloaded such that the initial value of the control action is equal to the nominal input $\overline{F_c}$. In the set-point following scenario a step change of amplitude $\Delta\overline{T_{po}}$ is added to $\overline{T_{po}}(t)$ at time zero. As regards disturbance rejection, three different scenarios are considered where a step disturbance is applied at time zero to $T_{ci}(t)$, $T_{pi}(t)$ and $F_p(t)$, respectively. The first one consists of a step disturbance of amplitude ΔT_{ci} that

is added to $\overline{T_{ci}}$. The second one consists of a step disturbance of amplitude ΔT_{pi} that is added to $\overline{T_{pi}}$. The last one consists of a step disturbance of amplitude ΔF_p that is added to $\overline{F_p}$. For each scenario, three different values are considered for the steps, and their values are shown in Table 3.
The responses obtained for the set-point following task are shown in Figure 5 and the corresponding performance indexes are shown in 5. The responses obtained for the disturbance rejection task with respect to step disturbances in $T_{ci}(t)$, $T_{pi}(t)$ and $F_p(t)$ are shown in Figures 6, 7 and 8, respectively. The corresponding performance indexes are shown in Tables 6, 7 and 8, respectively. Note that, in the top plot of the figures, the $T_{po}(t)$ signal is shown. This it is the value of the process fluid outlet temperature not affected by the measurement noise. This choice has been done to better highlight the different responses obtained by the two controllers. However, it is worth stressing that this is only a choice made for the sake of clarity in presenting the results. In fact, the variable $\widetilde{T_{po}}(t)$ is actually given to the controllers as the residual noise that affects the control action shown in the bottom plot testifies. Note that the two plots also have a different time scale to better highlight the differences in the control actions between the two controllers. The obtained results show that the PIDA controller provides an improved performance with respect to the PID controller. In particular, for all the considered simulation considered the PIDA controller provides a reduction of the IAE with respect to that obtained with the PID from a minimum of 4.68% to a maximum of 17.94%. As regards the time responses, this translates into a faster responses, in an improved damping of the oscillations and, thus, in a shorter settling time. The performance improvement is paid at the cost of slightly higher values of the control action. In particular, it is possible to note that the PIDA controller provides faster changes in the control action thanks to the presence of the acceleration term. However, this is not paid at the cost of acceleration kicks and also the noise is filtered very effectively. This can be checked by observing that the amount of residual noise affecting the control action is small. Finally, it is worth noting that, for both controllers, the control performance degrade as the amplitude of the set-point changes and of the disturbances increase. This is due to the fact that, as the amplitude of these signal increases, the distance from the nominal operating point also increases but the linearized models used to tune the controllers are well representative of the process behavior only for small deviations from the nominal operating point. Interestingly, the PIDA controller provides greater performance improvements with respect to the PID controller as the distance from the nominal operating conditions increases. This means that the PIDA controller can provide an improved robustness with respect to the PID controller, thus allowing a satisfactory control performance to be obtained over a wider range of operating conditions.

Table 3: Values of the step changes considered in each simulation scenario.

	Set-point	**Disturbance**		
	$\Delta\overline{T_{po}}$ [K]	ΔT_{ci} [K]	ΔT_{pi} [K]	ΔF_p [kg/s]
Case 1	+5	-5	-5	-0.025
Case 2	+2.5	-2.5	-2.5	-0.012
Case 3	-2.5	2.5	2.5	+0.012

Table 4: Tuning parameters values of the controllers employed in the simulations.

	K_p	T_i	T_d	T_a	T_f
PIDA	-0.021	47.53	12.85	49.98	5.10
PID	-0.018	42.42	10.60	0	5.46

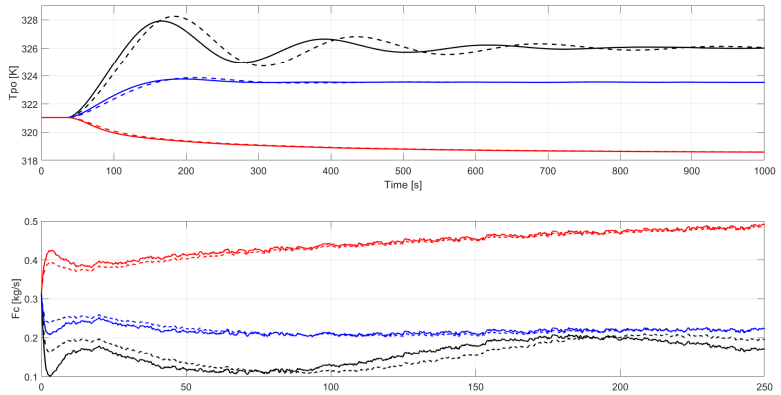

Figure 5: Set-point following responses obtained to step changes in $\overline{T_{po}}(t)$ of amplitudes $\Delta\overline{T_{po}}(t)$ = +5 K (black lines), $\Delta\overline{T_{po}}(t)$ = +2.5 K (blue lines) and $\Delta\overline{T_{po}}(t)$ = -2.5 K (red lines) applied at time zero. Solid lines: PIDA controller. Dashed lines: PID controller.

Table 5: Set-point following performance indexes obtained to step changes in $\overline{T_{po}}(t)$.

$\Delta\overline{T_{po}}$ [K]	IAE_{PID}	IAE_{PIDA}	Δ_{IAE} [%]
+5	865.03	709.78	17.94
+2.5	285.75	251.14	12.11
-2.5	552.60	525.67	4.87

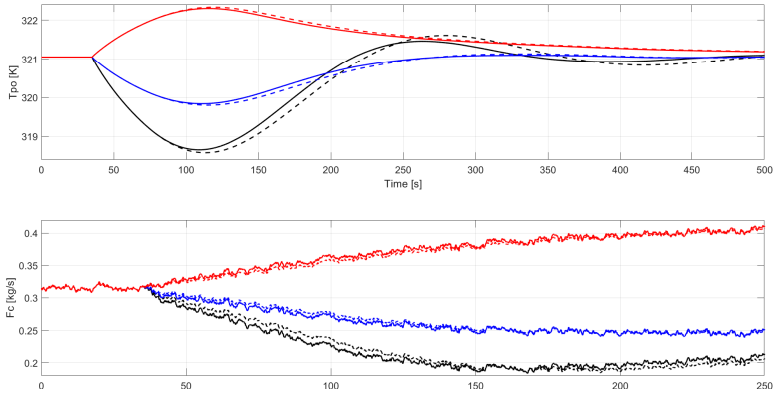

Figure 6: Disturbance rejection responses obtained to step changes in $T_{ci}(t)$ of ΔT_{ci} = -5 K (black lines), ΔT_{ci} = -2.5 K (blue lines) and ΔT_{ci} = +2.5 K (red lines) applied at time zero. Solid lines: PIDA controller. Dashed lines: PID controller.

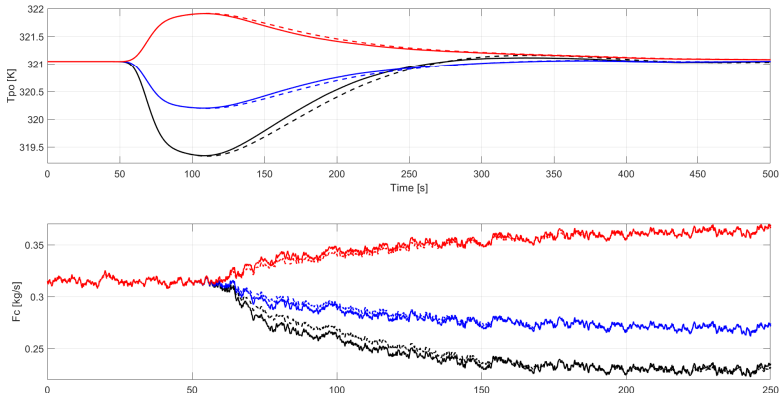

Figure 7: Disturbance rejection responses obtained to step changes in $T_{pi}(t)$ of ΔT_{pi} = -5 K (black lines), ΔT_{pi} = -2.5 K (blue lines) and ΔT_{pi} = +2.5 K (red lines) applied at time zero. Solid lines: PIDA controller. Dashed lines: PID controller.

Table 6: Disturbance rejection performance indexes obtained to step changes in $T_{ci}(t)$.

ΔT_{ci} [K]	IAE_{PID}	IAE_{PIDA}	Δ_{IAE} [%]
-5	349.25	302.86	13.28
-2.5	169.81	154.89	8.79
+2.5	264.84	252.46	4.68

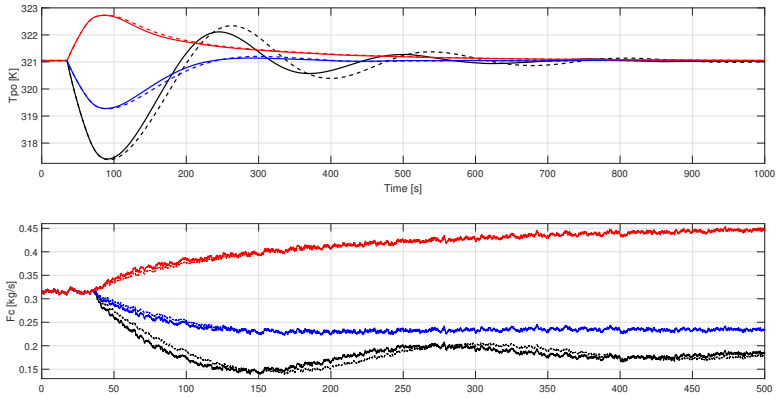

Figure 8: Disturbance rejection responses obtained to step changes in $F_p(t)$ of ΔF_p = -0.025 kg/s (black lines), ΔF_p = -0.012 kg/s (blue lines) and ΔF_p = +0.012 kg/s (red lines) applied at time zero. Solid lines: PIDA controller. Dashed lines: PID controller.

Table 7: Disturbance rejection performance indexes obtained to step changes in $T_{pi}(t)$.

ΔT_{pi} [K]	IAE_{PID}	IAE_{PIDA}	Δ_{IAE} [%]
-5	211.60	192.55	9.00
-2.5	108.16	101.44	6.21
+2.5	133.75	126.89	5.13

Table 8: Disturbance rejection performance indexes obtained to step changes in $F_p(t)$.

ΔF_p [K]	IAE_{PID}	IAE_{PIDA}	Δ_{IAE} [%]
-0.025	606.94	506.47	16.55
-0.012	223.62	201.33	9.97
+0.012	329.01	311.97	5.18

5 Conclusions

In this paper the performance improvement achievable with a PIDA controller compared to a conventional PID controller when applied to a realistic heat exchanger simulator is evaluated. The results obtained in this study demonstrate that the PIDA controller provides a performance improvement in both set-point following and disturbance rejection tasks, as witnessed by a reduction of the IAE ranging from 4.68% to 17.94%. This translates into faster responses, enhanced damping of oscillations, and shorter settling times. The PIDA controller is able to increase robustness, maintaining a satisfactory performance even under larger deviations from nominal operating conditions. These findings confirmed that the benefits of PIDA control extend even on systems characterized by a strong nonlinear behavior, such as heat exchangers, thus highlighting its effectiveness also in this context. Notably, the advantages offered by the PIDA controller over PID control are achieved without significantly increasing the controller complexity or the tuning efforts, thus offering a cost-effective means to enhance operational efficiency.

Acknowledgments


Funded by the European Union under GA No 101115601 (PUSH-CCC). Views and opinions expressed are however those of the author(s) only and do not necessarily reflect those of the European Union or EISMEA. Neither the European Union nor the granting authority can be held responsible for them.

References

[1] G. Alva, Y. Lin, and G. Fang, "An overview of thermal energy storage systems," *Energy*, vol. 144, pp. 341–378, 2018.

[2] M. A. Abdelghani-Idrissi, M. A. Arbaoui, L. Estel, and J. Richalet, "Predictive functional control of a counter current heat exchanger using convexity property," *Chemical Engineering and Processing: Process Intensification*, vol. 40, no. 5, pp. 449–457, 2001.

[3] A. Pacheco-Vega, C. Ruiz-Mercado, K. Peters, and L. E. Vilchiz, "Online fuzzy-logic-based temperature control of a concentric-tube heat exchanger facility," *Heat Transfer Engineering*, vol. 30, no. 14, pp. 1208–1215, 2009.

[4] J. Oravec, M. Bakošová, M. Trafczynski, A. Vasičkaninová, A. Mészáros, and M. Markowski, "Robust model predictive control and

PID control of shell-and-tube heat exchangers," *Energy*, vol. 159, pp. 1–10, 2018.

[5] A. Vasičkaninová, M. Bakošová, L. Čirka, M. Kalúz, and J. Oravec, "Robust controller design for a laboratory heat exchanger," *Applied Thermal Engineering*, vol. 128, pp. 1297–1309, 2018.

[6] M. Milanesi, E. Mirandola, and A. Visioli, "A comparison between PID and PIDA controllers," in *Proceedings 27th International Conference on Emerging Technologies and Factory Automation*, Stuttgart, D, 2022.

[7] M. Huba, "Filtered PIDA controller for the double integrator plus dead time," in *Proceedings 16th IFAC Conference on Programmable Devices and Embedded Systems*, High Tatras, SK, 2019, pp. 106–113.

[8] M. Huba, D. Vrancic, and P. Bistak, "PID control with higher order derivative degrees for IPDT plant models," *IEEE Access*, vol. 9, pp. 2478–2495, 2021.

[9] A. Visioli and J. Sanchez-Moreno, "Design of PIDA controllers for high-order integral processes," in *Proceedings 28th International Conference on Emerging Technologies and Factory Automation*, Sinaia, RO, 2023.

[10] P. Bistak, M. Huba, D. Vrancic, and S. Chamraz, "IPDT model-based Ziegler–Nichols tuning generalized to controllers with higher-order derivatives," *Sensors*, vol. 23, no. 8, 2023.

[11] M. Huba, P. Bistak, and D. Vrancic, "Parametrization and optimal tuning of constrained series PIDA controller for IPDT models," *Mathematics*, vol. 11, no. 20, 2023.

[12] ——, "Series PIDA controller design for IPDT processes," *Applied Sciences*, vol. 13, no. 4, 2023.

[13] ——, "Optimizing constrained series PIDA controller for speed loops inspired by Ziegler-Nichols," in *Proceeding International Conference on Electrical Drives and Power Electronics*, 2023.

[14] M. Huba, D. Vrancic, and P. Bistak, "Series PID control with higher-order derivatives for processes approximated by IPDT models," *IEEE Transactions on Automation Science and Engineering*, pp. 1–13, 2023.

[15] A. Visioli and J. Sanchez-Moreno, "A relay-feedback automatic tuning methodology of PIDA controllers for high-order processes," *International Journal of Control*, vol. 97, no. 1, pp. 51–58, 2024.

[16] F. Campregher, M. Milanesi, M. Schiavo, and A. Visioli, "Generalized haalman tuning of PIDA controllers," in *Proceedings IFAC Conference on Advances in PID Control*, Almeria, E, 2024.

[17] J. Sanchez, S. Dormido, and J. M. Diaz, "Fitting of generic process models by an asymmetric short relay feedback experiment— the n-shifting method," *Applied Sciences*, vol. 11, no. 4, p. 1651, 2021.

[18] A. W. Alsop and T. F. Edgar, "Nonlinear heat exchanger control through the use of partially linearized control variables," *Chemical Engineering Communications*, vol. 75, no. 1, pp. 155–170, 1989.

[19] R. Sanchis and I. Peñarrocha-Alós, "A new method for experimental tuning of PI controllers based on the step response," *ISA Transactions*, vol. 128, pp. 329–342, 2022.

[20] K. J. Åström and T. Hägglund, *Advanced PID Control*. Research Triangle Park, USA: ISA Press, 2006.

[21] M. Veronesi, R. D. Keyser, R. Vilanova, and A. Visioli, "Estimation of a SOPDT process transfer function for PID tuning," in *Proceedings IFAC Conference on Advances in PID Control*, Almeria, E, 2024.